


Explaining the AMS positron excess via right-handed neutrinos

Farinaldo S. Queiroz^{*} and Clarissa Siqueira[†]

*International Institute of Physics, Universidade Federal do Rio Grande do Norte,
Campus Universitario, Lagoa Nova, Natal-RN 59078-970, Brazil*

 (Received 31 October 2019; accepted 16 March 2020; published 6 April 2020)

We have witnessed in the past decade the observation of a puzzling cosmic-ray excess at energies larger than 10 GeV. The AMS-02 data published this year have new ingredients such as the bump around 300 GeV followed by a drop at 800 GeV, as well as smaller error bars. Adopting the background used by the AMS-02 Collaboration in their analysis, one can conclude that previous explanations to the new AMS-02 such as one component annihilating and decaying dark matter as well as pulsars seem to fail at reproducing the data. Here, we show that in the right-handed neutrino portal might reside the answer. We discuss a decaying two-component dark matter scenario where the two-body decay products are right-handed neutrinos that have their decay pattern governed by the type-I seesaw mechanism. This setup provides a very good fit to the data; for example, a conservative approach including just statistical uncertainties leads to $\chi^2/\text{DOF} \sim 2.3$ for $m_{DM_1} = 2150$ GeV with $\tau_1 = 3.78 \times 10^{26}$ s and $m_{DM_2} = 300$ with $\tau_2 = 5.0 \times 10^{27}$ s for $M_N = 10$ GeV, and, in an optimistic case, including systematic uncertainties, we find $\chi^2/\text{DOF} \sim 1.12$, for $M_N = 10$ GeV, with $m_{DM_1} = 2200$ GeV with $\tau_1 = 3.8 \times 10^{26}$ s and $m_{DM_2} = 323$ GeV with $\tau_2 = 1.68 \times 10^{27}$ s.

DOI: [10.1103/PhysRevD.101.075007](https://doi.org/10.1103/PhysRevD.101.075007)

I. INTRODUCTION

The observation of cosmic rays has boosted our understanding of astrophysical phenomena that undergo diffusion and energy loss processes in the intergalactic medium. Historically, in 2008 the payload for antimatter matter exploration and light-nuclei astrophysics (PAMELA) surprisingly announced the first evidence of a rise in the cosmic-ray positron fraction at GeV energies with high statistics [1]. Fermi-LAT confirmed this cosmic-ray anomaly much later in 2011. Taking advantage of the absent onboard magnet, they could distinguish electrons from positrons by exploiting Earth's shadow, which is offset in opposite directions for opposite charges due to Earth's magnetic field. With this technique, they were able to indeed observe a positron fraction rise for energies between 20 and 200 GeV [2]. With much better statistics, the AMS mission measured the positron fraction up to 350 GeV [3] and reported a flat positron fraction for energies above 150 GeV.

That has triggered a number of works which were able to explain the AMS excess of events. Some attempts focused on annihilating dark matter [4,5], but the annihilation cross section needed to fit the excess was too large to be in agreement with gamma-ray observations in the direction of the Galactic center and dwarf spheroidal galaxies [6,7] and cosmic microwave background data [8,9]. Interpretations in terms of decaying dark matter were also put forth, where a lifetime of the order of 10^{27} s for $\mu\bar{\mu}$ final states could provide a reasonable fit to the data [10–14]. Alternatively, nearby astrophysical objects presented themselves as good candidates [15–17]. That was the whole story until the new AMS data and High-Altitude Water Cherenkov Observatory (HAWC) observations came into light.

The new AMS data have new ingredients [18]: (i) features much smaller error bars at low energies and a rise at ~ 10 GeV; (ii) the previously observed flat spectrum for energies larger than 150 GeV now exhibits a bump-like feature with a peak around 300 GeV; (iii) a sharp drop for energies above 400 GeV is visible. These new ingredients significantly harden the shape of the spectrum, making a dark matter interpretation difficult, especially adopting the single-component scenario. Moreover, the HAWC observed the presence of energetic electrons and positrons from nearby pulsars, and from that the diffusion parameters were inferred. The diffusion parameters derived are inconsistent with the one observed by AMS-02 though, thus ruling out such pulsars as the origin of the AMS excess [19]. In conclusion, the new AMS data beg for a new interpretation [20].

^{*}farinaldo.queiroz@iip.ufrn.br
[†]csiqueira@iip.ufrn.br

Published by the American Physical Society under the terms of the Creative Commons Attribution 4.0 International license. Further distribution of this work must maintain attribution to the author(s) and the published article's title, journal citation, and DOI. Funded by SCOAP³.

In this work, we attempt to explain the positron excess in terms of two-component dark matter comprised of two scalars. Such scalars decay into two right-handed neutrinos that decay into Standard Model (SM) particles according to the type-I seesaw mechanism [21,22]. This scenario appears in Majoron-inspired models, for instance, Refs. [23–33]. We emphasize that, in the canonical Majoron model, the decay into right-handed neutrinos is not dominant. Decays into left-handed neutrinos are instead more relevant, and they lead to an interesting phenomenology explored elsewhere [32]. In this work, we are investigating the possibility of fitting the AMS-02 data with a two-component dark matter setup, where each component decays into two right-handed neutrinos. We are not interested in a explicit theoretical realization of this scenario, but we do emphasize that having a two-component decay dark matter model requires going beyond the vanilla Majoron models and other type-I seesaw model incarnations. Our idea is simply to assess whether one could get a reasonable fit to the AMS-02 data if such decays are dominant, without having a specific model at hand.

That said, we perform a chi-squared analysis choosing different masses for the right-handed neutrino (10, 50, and 80 GeV) and leaving the dark matter (DM) mass and the decay rate as free parameters to get the best fit to the data. In addition, we choose two different set of propagation parameters which are known as *medium* (MED) and *maximum* (MAX) diffusion models, using the Navarro-Frenk-White (NFW) profile.

Moreover, we carry out all this procedure including only statistical errors and statistical plus systematic errors to really assess the impact of the systematic effects on our conclusions. Including only the statistical uncertainties, we find the best fit of $\chi^2/\text{DOF} \sim 2.3$ for $m_{DM_1} = 300$ with $\tau_1 = 1.67 \times 10^{27}$ s and $m_{DM_2} = 2000$ GeV with $\tau_{DM_2} = 4 \times 10^{26}$ s for $M_N = 10$ GeV, and, for the optimistic case, including systematic uncertainties, we get $\tau_1 = 1.68 \times 10^{27}$ s and $\tau_{DM_2} = 3.8 \times 10^{26}$ s, for $m_{DM_1} = 323$ GeV and $m_{DM_2} = 2200$ GeV, respectively, with $M_N = 10$ GeV, yielding $\chi^2/\text{DOF} \sim 1.12$.

Last, we put our results into perspective with gamma-ray observations [34,35]. We start our reasoning discussing below how we obtain the positron flux.

II. POSITRON FLUX

The positron flux reported by AMS seems to be compatible with a background, which is given by a diffuse flux at low energies and a new source at high energies. So, the collaboration interpreted the whole signal as a background plus a new source term as follows:

$$\Phi_{\text{tot}}^{e^+} = \Phi_{\text{diffuse}}^{e^+} + \Phi_{\text{source}}^{e^+}. \quad (1)$$

In this work, we choose decaying dark matter particles to be responsible for this new source flux, $\Phi_{\text{source}}^{e^+}$, described

above. For this purpose, it is necessary to compute the decaying DM positron flux, which is given by

$$\Phi_{DM}^{e^+}(E) = \frac{1}{4\pi b(E) m_{DM}} \rho_{\odot} \Gamma \times \int_E^{m_{DM}/2} dE_s \sum_f BR_f \frac{dN_f^{e^+}}{dE}(E_s) \mathcal{I}(E, E_s), \quad (2)$$

where E is the positron energy after propagation and E_s is the positron energy at production, $\rho_{\odot} = 0.4 \text{ GeV/cm}^3$ is the DM density in the location of the Sun, m_{DM} is the DM mass, Γ is the decay rate of the DM particle, BR_f is the branching ratio for a given final state f , and $\frac{dN_f^{e^+}}{dE}(E_s)$ is the number of positrons per energy produced after decay before the propagation. The parameter $b(E)$ is the called energy loss function, which takes into account the possible energy losses via synchrotron radiation and inverse Compton scattering.

For the purpose of being conservative, we choose the same diffuse flux as reported by the collaboration, which includes contributions from the interaction between Galactic cosmic rays with the intergalactic medium:

$$\Phi_{\text{diffuse}}^{e^+}(E) = c_d \frac{E^2}{\hat{E}^2} \left(\frac{\hat{E}}{E_1} \right)^{\gamma_d}, \quad (3)$$

where the values for the parameters reported by the collaboration were $E_1 = 7 \text{ GeV}$, $\hat{E}(E) = E + \varphi_{e^+}$, with $\varphi_{e^+} = 1.10 \pm 0.03 \text{ GeV}$, $c_d = (6.51 \pm 0.14) \times 10^{-2} (\text{m}^2 \text{srs GeV})^{-1}$, and $\gamma_d = -4.07 \pm 0.06$, where we use the central values for the parameters E_1 and φ_{e^+} , while the values for c_d and γ_d were chosen within 3σ contour in order to provide the best fit to the data.

Furthermore, the halo function $\mathcal{I}(E, E_s)$, computed using the numerical package PPC4DMID, appears as a solution to the diffusion equation, and it is dependent on the loss energy function [$b(E)$], on the DM profile (here we choose the NFW), on the diffusion parameters $\mathcal{K}_0 = 0.0112 \text{ kpc}^2/\text{Myr}$ and $\delta = 0.70$ for the medium (MED) and $\mathcal{K}_0 = 0.0765 \text{ kpc}^2/\text{Myr}$ and $\delta = 0.46$ for the maximum (MAX) propagation models.

In the next section, we will compute the fluxes for the model considered here.

III. RESULTS

The scenario involves two DM particles decaying into two right-handed neutrino (RHN) pairs. We assume each DM candidate composing 50% of the DM abundance of the Universe, and, of course, these values can be easily changed by rescaling the decay rate accordingly. These RHN couples to Standard Model particles via Higgs and gauge bosons, leading to the following RHN decay pattern: $N_R \rightarrow W^{\pm} + l^{\mp}$, $N_R \rightarrow Z + \nu_l$, and $N_R \rightarrow H + \nu_l$, where, in principle, l can be the three leptonic flavors, but in our case, for simplicity, we choose $l = e$. In addition, we impose three different values for the RHN mass: $M_N = 10 \text{ GeV}$, $M_N = 50 \text{ GeV}$, and $M_N = 80 \text{ GeV}$.

TABLE I. Background parameters used in each analysis within 3σ uncertainties. The values were chosen in order to get the best values for the χ^2/DOF .

Propagation model	M_N (GeV)	c_d ($\text{m}^2 \text{sr s GeV}^{-1}$)	γ_d
MED	10	6.4×10^{-2}	-4.02
	50	6.2×10^{-2}	-4.00
	80	6.3×10^{-2}	-4.00
MAX	10	6.4×10^{-2}	-4.02
	50	6.1×10^{-2}	-3.97
	80	6.0×10^{-2}	-3.98

Fixing the RHN masses, we compute the positron flux in Eq. (2) using the PPPC4DMID code, which computes the halo function $\mathcal{I}(E, E_s)$, and the PYTHIA8 package to obtain the

positron spectrum for each right-handed neutrino mass. Then we left as free parameters the DM masses M_{DM_1} and M_{DM_2} and the decay rates in order to fit the data reported by the AMS Collaboration; namely, for each RHN mass, we found a combination of DM mass versus decay rate which provides the best fit for the data.

To be conservative, in these first analyses, we compute the goodness of the fit, χ^2/DOF , using only the statistical uncertainties provided by the collaboration. For each scenario, we chose the best values within 3σ error for the parameters c_d and γ_d to get the best values for the fit, according to Table I.

In Figs. 1–3, we present the computed fluxes including that predicted by each decaying DM component (continuous and dashed lines), the background contribution (gray

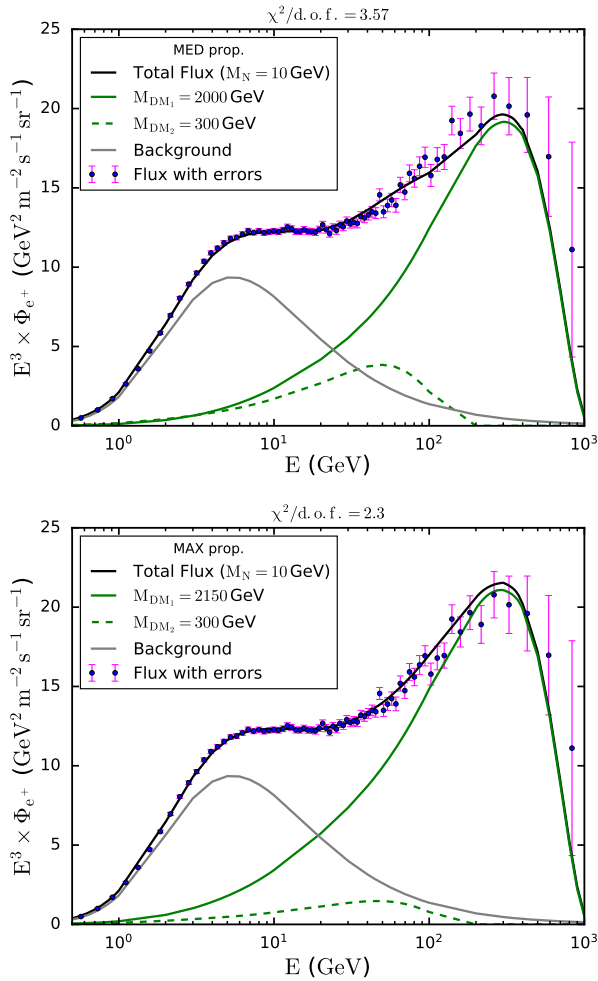


FIG. 1. Positron flux versus energy, summing over different contributions (black line): dark matter candidate 1 (continuous green line), dark matter candidate 2 (dashed green line), and diffuse background (gray line). In this case, we choose the right-handed neutrino mass equal to 10 GeV for two different propagation models, MED (top) and MAX (bottom), with $\chi^2/\text{DOF} = 3.57$ and $\chi^2/\text{DOF} = 2.3$, respectively.

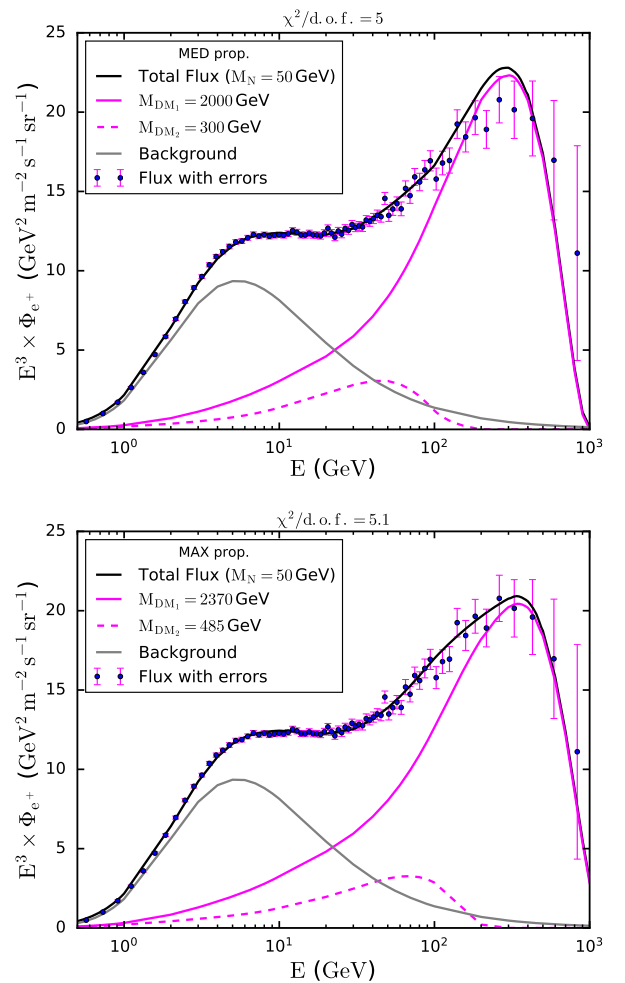


FIG. 2. Expected positron flux versus energy, summing over different contributions (black line): dark matter candidate 1 (continuous magenta line), dark matter candidate 2 (dashed magenta line), and diffuse background (gray line). In this case, we choose the right-handed neutrino mass equal to 50 GeV, for two different propagation models, MED (top) and MAX (bottom), with $\chi^2/\text{DOF} = 5$ and $\chi^2/\text{DOF} = 5.1$, respectively.

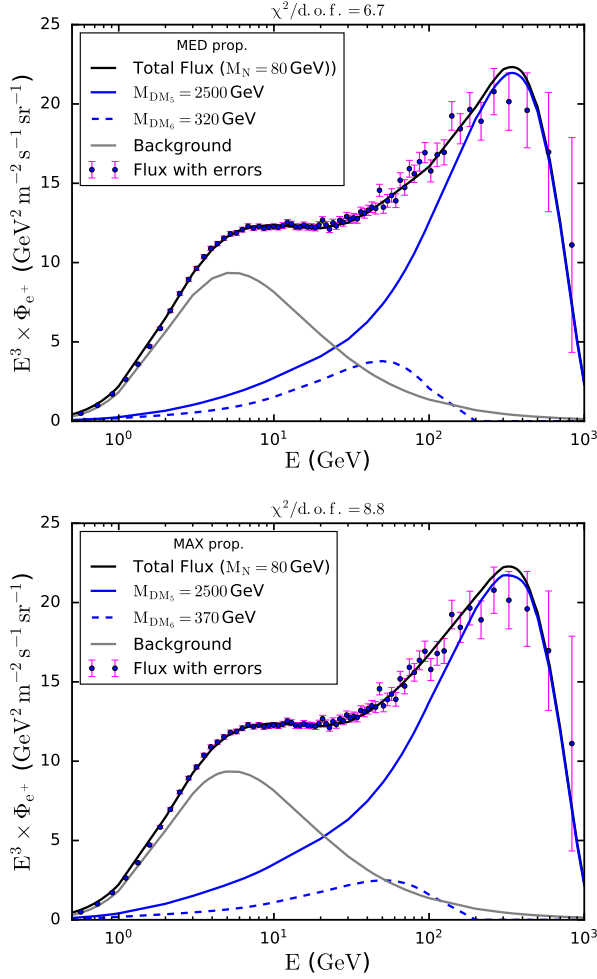


FIG. 3. Expected positron flux summing over different contributions (black line): dark matter candidate 1 (continuous blue line), dark matter candidate 2 (dashed blue line), and diffuse background (gray line). In this case, we choose the right-handed neutrino mass equal to 80 GeV, for two different propagation models, MED (top) and MAX (bottom), with $\chi^2/\text{DOF} = 6.7$ and $\chi^2/\text{DOF} = 8.8$, respectively.

lines), and the sum over all components (black lines). The AMS data [18] are also shown for comparison.

In Fig. 1, we show our results for $M_N = 10$ GeV for two different propagation models, MED and MAX (top and bottom, respectively). We found the best fit value equal to $\chi^2/\text{DOF} = 3.57$ for the MED propagation model and $\chi^2/\text{DOF} = 2.3$ for the MAX propagation. In Table I, we include the background parameters c_d and γ_d adopted for each scenario.

In Fig. 2, we show our results taking $M_N = 50$ GeV for two different propagation models, MED and MAX, following the same description above. We found the best fit value equal to $\chi^2/\text{DOF} = 5.0$ for the MED propagation model and $\chi^2/\text{DOF} = 5.1$ for the MAX propagation. For $M_N = 80$ GeV, we found $\chi^2/\text{DOF} = 6.7$ (8.8) for MED (MAX) propagation (Fig. 3).

TABLE II. Best-fit parameters found for the different scenarios.

Propagation model	M_N (GeV)	M_{DM_1} (GeV)	τ_1 (s)	M_{DM_2} (GeV)	τ_2 (s)	χ^2/DOF
MED	10	2000	4.00×10^{26}	300	1.67×10^{27}	3.57
	50	2000	3.35×10^{26}	300	2.00×10^{27}	5.0
	80	2500	3.34×10^{26}	320	1.80×10^{27}	6.7
MAX	10	2150	3.78×10^{26}	300	5.00×10^{27}	2.3
	50	2370	4.07×10^{26}	485	2.20×10^{27}	5.1
	80	2500	3.60×10^{26}	370	3.00×10^{27}	8.8

Summarizing, in Table II we show the best-fit values found for the parameters DM mass and lifetime for each DM candidate in order to get the best fit to the data. In Figs. 4 (MED propagation) and 5 (MAX propagation), we present the 1σ , 2σ , and 3σ contours for both DM1 (top) and DM2 (bottom) candidates following the same color pattern for the RHN masses described above.

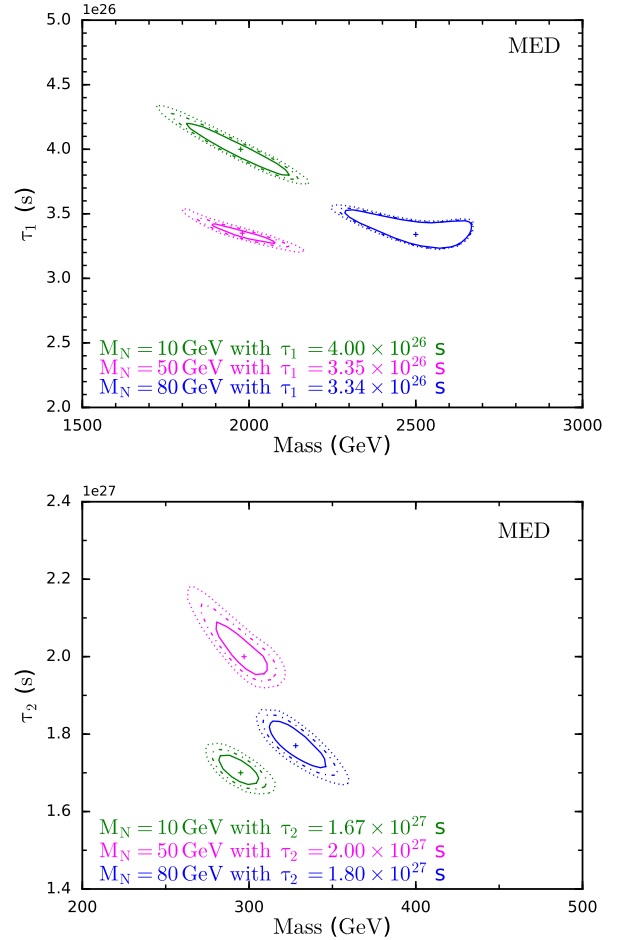


FIG. 4. 1σ (continuous lines), 2σ (dashed lines), and 3σ (dotted lines) regions for dark matter candidate 1 (top) and for dark matter candidate 2 (bottom) for different right-handed neutrino masses, for $M_N = 10$ GeV (green), $M_N = 50$ GeV (magenta), and $M_N = 80$ GeV (blue).

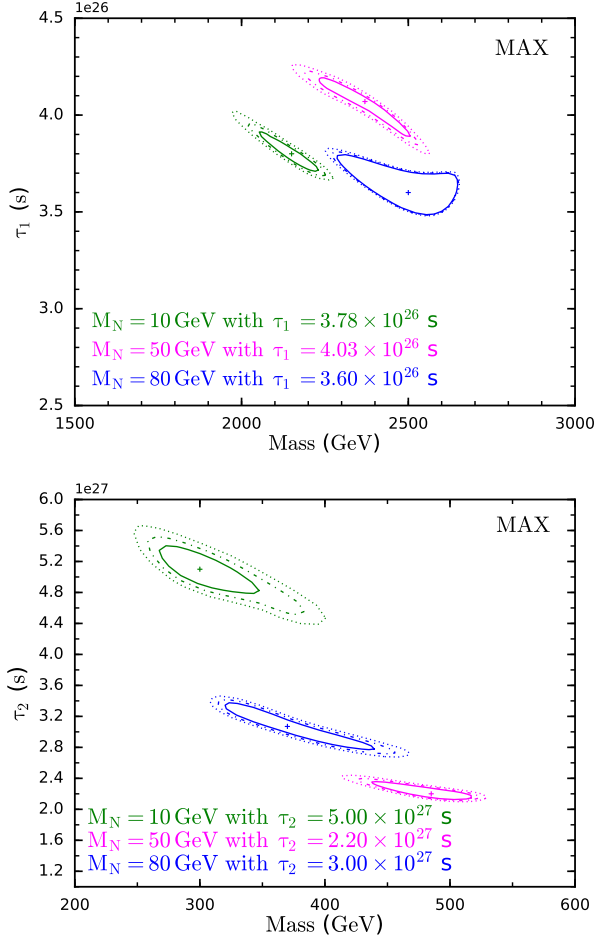


FIG. 5. 1σ (continuous lines), 2σ (dashed lines), and 3σ (dotted lines) regions for dark matter candidate 1 (top) and for dark matter candidate 2 (bottom) with different right-handed neutrino masses, for $M_N = 10$ GeV (green), $M_N = 50$ GeV (magenta), and $M_N = 80$ GeV (blue).

As we can see, the larger the right-handed neutrino mass, the worse the fit to the data. This is due to the change in the shape of the spectrum. Although their shapes seem to be quite similar, minimum modifications in the tail (lower energies) provide a significant impact on the χ^2/DOF as a result of the smallness of the error bars at lower energies.

In the same way, the MED propagation model yields smaller fluxes than the MAX propagation one. Hence, we can play with the decay rate (or lifetime) in order to obtain similar fits for both propagation models. For example, taking $M_N = 10$ GeV, the best fit is found for $\tau_2 = 1.67 \times 10^{27}$ s and $M_{DM_2} = 300$ GeV for MED propagation, while for MAX we need 5.0×10^{27} s (see Table II). As the MAX model gives rise to the steeper energy spectrum, we need to increase the lifetime to find a similar fit.

The combination of two different candidates can provide an excellent agreement with the AMS excess, including one of them with a mass around hundreds of GeV and another with a mass of a few TeV. It is worth emphasizing that the

choice 50%–50% for each DM candidate is arbitrary, in a way that modification of this percentage results simply in a rescaling of the lifetime.

A. Including systematic uncertainties

The previous analysis included just statistical uncertainties which can be considered conservative, as the interpretation of the AMS data is dominated by systematics. Here, we include systematic uncertainties in order to verify its impact in the limits. We concluded that the main impact occurs at lower energies which feature rather small error bars. Therefore, the impact in the χ^2/DOF can be large but usually decreases by a factor of a few. In our study, we choose the MED propagation, with systematic uncertainties provided by the collaboration [18]. One can easily realize that the choice for MED or MAX propagation model does not result in significant changes to our conclusions, and for this reason we chose to focus on the MED model in this particular analysis. We emphasize that our conclusions would still apply for the MAX propagation model. We repeat the procedure above and assume that each dark matter particle contributes to 50% of the dark matter density.

In Fig. 6, we present the fluxes that yield the best fit for $M_N = 10$ GeV. As shown in Fig. 6, we obtained $M_{DM_1} = 2200$ GeV (green continuous line) and $M_{DM_2} = 323$ GeV (green dashed line). The diffuse flux (gray line) and total flux (black line) are also exhibited. This setup results in $\chi^2/\text{DOF} = 1.12$.

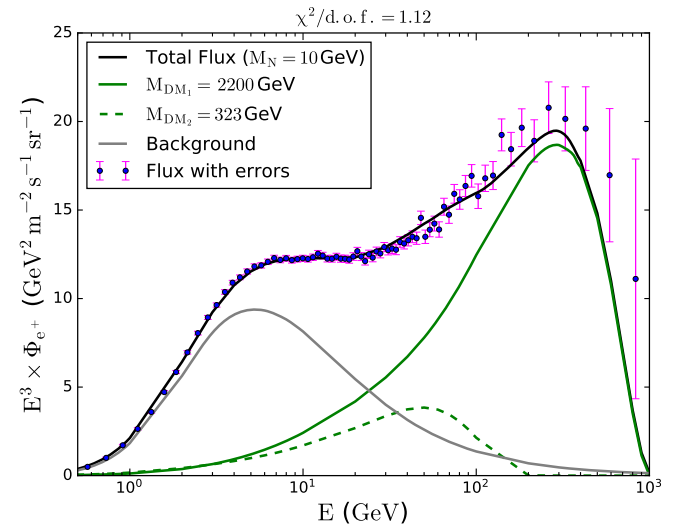


FIG. 6. Expected positron flux versus energy, summing over different contributions (black line): dark matter candidate 1 (dashed line), dark matter candidate 2 (continuous line), and diffuse background (gray line). In this case, we choose the right-handed neutrino mass equal to 10 GeV, and we found $\chi^2/\text{DOF} = 1.12$.

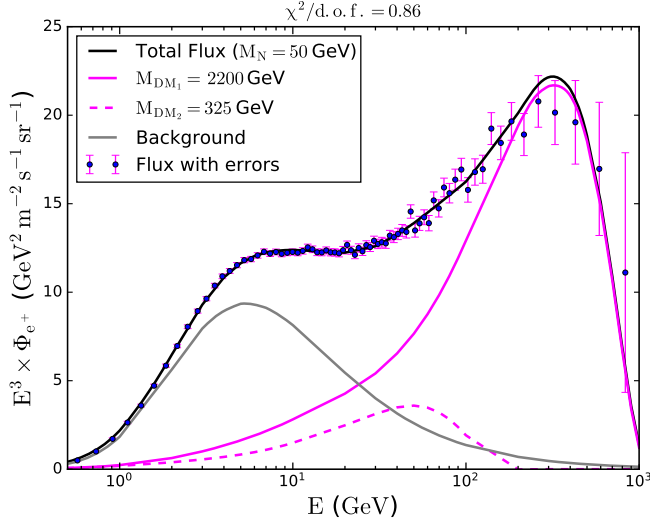


FIG. 7. Expected positron flux versus energy, summing over different contributions (black line): dark matter candidate 1 (dashed line), dark matter candidate 2 (continuous line), and diffuse background (gray line). In this case, we choose the right-handed neutrino mass equal to 50 GeV, and we found $\chi^2/\text{DOF} = 0.86$.

In Fig. 7, we exhibit our results assuming $M_N = 50$ GeV. The best-fit point yields $\chi^2/\text{DOF} = 0.86$, and it is found for $M_{DM_1} = 2200$ GeV (pink continuous line) and $M_{DM_2} = 323$ GeV (pink dashed line).

In Fig. 8, we repeat the exercise for $M_N = 80$ GeV, which still provides a good fit to the data with $\chi^2/\text{DOF} = 1.06$ for $M_{DM_1} = 2350$ GeV (blue continuous line) and $M_{DM_2} = 327$ GeV (blue dashed line).

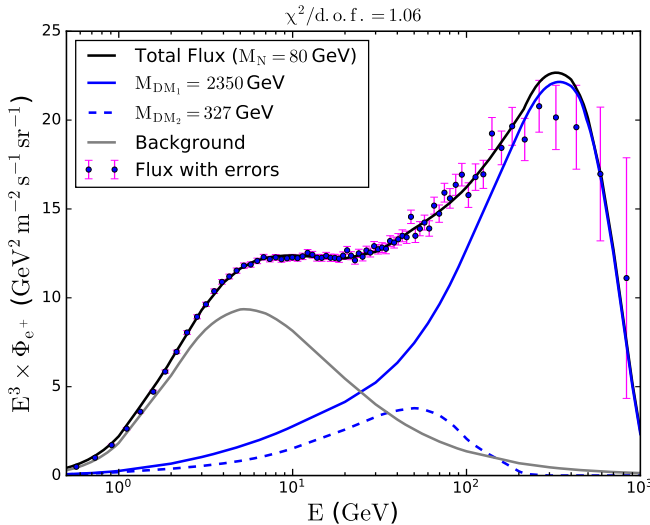


FIG. 8. Expected positron flux versus energy, summing over different contributions (black line): dark matter candidate 1 (solid line), dark matter candidate 2 (dashed line), and diffuse background (gray line). In this case, we choose the right-handed neutrino mass equal to 80 GeV, and we found $\chi^2/\text{DOF} = 1.06$.

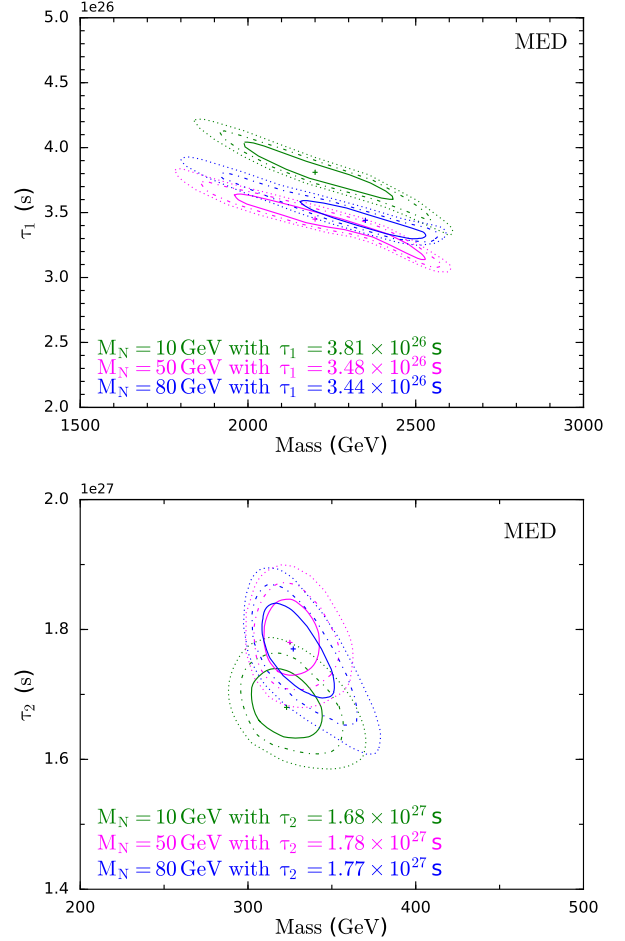


FIG. 9. 1σ (continuous lines), 2σ (dashed lines), and 3σ (dotted lines) regions for dark matter candidate 1 (top) and for dark matter candidate 2 (bottom) with different right-handed neutrino masses, for $M_N = 10$ GeV (green), $M_N = 50$ GeV (magenta), and $M_N = 80$ GeV (blue).

We have explicitly shown that our benchmark scenarios provide a good fit to the data and now display the best-fit contours [1σ (continuous lines), 2σ (dashed lines), and 3σ (dotted lines) contours] in terms of the lifetime and dark matter mass in Fig. 9 for each setup discussed, where both statistical and systematic errors are included.

One could find that the best fit is found for $M_N = 50$ GeV; however, since the AMS data are driven by systematic errors, it is reasonable to conclude that all of them provide an equally good fit to the data. For concreteness, we computed the p value, and we found, for instance, including systematic uncertainties, p value = 0.25 for $M_N = 10$ GeV, p value = 0.78 for $M_N = 50$ GeV, and p value = 0.33 for $M_N = 80$ GeV. Thus, we did find a good fit to the data. However, we would like to stress that the statistical method used is not of utmost importance, because the AMS-02 data are driven by systematics.

IV. DISCUSSION

The two-component dark matter scenario where a scalar (or vector) decays into a right-handed neutrino pair was motivated by scalar models which embed the type-I seesaw mechanism. In the type-I seesaw mechanism, the right-handed neutrinos are typically very heavy; however, we found that for masses heavier than ~ 100 GeV the fit to the AMS data becomes quite poor. This can be understood via the energy spectrum. When right-handed neutrinos are heavier than 100 GeV, the decay channels into Z and W bosons are open, leading to significant changes in the energy spectrum, and, as we checked, it provides a poor fit to the data. That said, even in the type-I seesaw mechanism, we can easily assume right-handed neutrino masses between 10 and 80 GeV by tuning the Yukawa couplings, bringing no changes to the branching ratio pattern, which justifies our analysis.

Another aspect of our study is the compatibility with limits stemming from gamma-ray data, because our decay channels also produce gamma rays. Our setup involved dark matter decaying into right-handed neutrino pairs, where each right-handed neutrino might decay into leptons and quarks via off-shell W , Higgs, and Z bosons. Thus, as we have not fixed a final decay channel, it is not so simple to compare with other existing limits in the literature. Sifting the energy spectra produced by DM decay into SM particles, we realized that the gamma-ray spectrum produced by a direct DM decay into WW and $W\ell$, though different, yields the closest shape to the energy spectra produced by our setup. Thus, we can compare the energy spectra and notice how much different they are and then rescale our energy spectra by a given amount to match the energy spectra of the WW and $W\ell$ channels. In this way, we may roughly estimate whether our benchmark points are in agreement with existing gamma-ray limits [36]. We concluded that, taking into account the fact that we have a two-component dark matter setup and the uncertainties involved in the gamma-ray limits, our benchmark points are consistent with the existing gamma-ray bounds. Although we highlight that there are no existing gamma-ray limits directly applicable to our model and that required an extra effort from our side to somehow compare our results with gamma-ray probes that feature a similar energy spectrum. We will prolong this discussion in the Appendix.

In summary, we have shown that such two-component dark matter via the right-handed neutrino portal offers a good fit to the data for right-handed neutrino masses between 10 and 80 GeV with the inclusion or not of systematic errors in the analysis. Within this mass range, the precise mass of the right-handed neutrino does not change much the lifetime and dark matter mass that best fit the data but does change the χ^2/DOF by a factor of 2. In addition to that, the change from the MED to the MAX propagation model does not bring significant changes to our study, despite the MAX propagation being recently

favored by recent observations of the boron-to-carbon ratio [37]. In our study, we concluded that masses around 300 GeV and 2 TeV with a lifetime of 4×10^{26} and 2×10^{27} s, respectively, are favored and marginally consistent with current bounds rising from gamma-ray observations.

V. CONCLUSIONS

The positron excess provided by the AMS Collaboration [18] remains an open question. In this work, we assessed a scenario where two decaying dark matter candidates may constitute an answer to the observed excess via the right-handed neutrino portal.

We have shown that DM particles decaying into right-handed neutrino pairs which couple to SM particles through Z , W , and Higgs bosons, inspired by the type-I seesaw mechanism, provide a very good fit to the data. For example, for a conservative approach including just statistical uncertainties, we got $\chi^2/\text{DOF} \sim 2.3$ for $m_{DM_1} = 2150$ GeV with $\tau_1 = 3.78 \times 10^{26}$ s and $m_{DM_2} = 300$ with $\tau_2 = 5.0 \times 10^{27}$ s for $M_N = 10$ GeV, and, in an optimistic case, including systematic uncertainties, we found $\chi^2/\text{DOF} \sim 1.12$, for $M_N = 10$ GeV, with $m_{DM_1} = 2200$ GeV with $\tau_1 = 3.8 \times 10^{26}$ s and $m_{DM_2} = 323$ GeV with $\tau_2 = 1.68 \times 10^{27}$ s.

Such benchmark points are consistent with existing gamma-ray bounds for lighter DM but in tension for heavier DM; however, as described in the Appendix, due to the large uncertainties in the gamma-ray limits, we may argue that our benchmarks are in agreement with gamma-ray data. It is important to emphasize that this is an estimate, and a careful analysis is needed. In addition, our benchmarks are significantly modified by changing the propagation model from MED to MAX. Knowing that the AMS results are dominated by systematics, our best-fit points might alter for a different assumption for the background. In our work, we adopted the background recommended by the AMS Collaboration.

In summary, we presented a plausible explanation for the puzzling AMS data via the right-handed neutrino portal.

ACKNOWLEDGMENTS

The authors thank Pasquale Serpico, Diego Restrepo, Manuela Vecchi, and Joseph Silk for useful discussions. F. S. Q. acknowledges support from CNPq Grants No. 303817/2018-6 and No. 421952/2018-0, UFRN, Ministério da Educação (MEC), and International Centre for Theoretical Physics/South American Institute for Fundamental Research (ICTPSAIFR) FAPESP Grant No. 2016/01343-7. C. S. thanks UFRN and for the financial support. We thank the High Performance Computing Center (NPAD) at UFRN for providing computational resources.

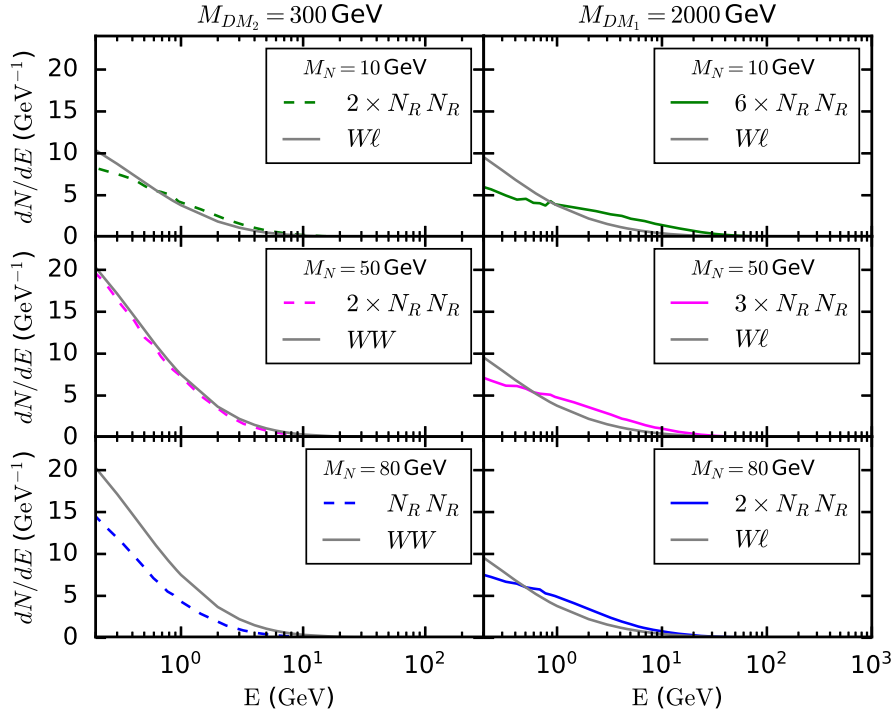


FIG. 10. Comparison between the gamma-ray spectrum provided by direct annihilations into WW and $W\ell$ with the spectrum provided by our right-handed neutrinos rescaled accordingly. For details, please see the text.

APPENDIX: COMPARISON WITH GAMMA-RAY DATA

The decay into right-handed neutrinos also produces gamma rays; thus, we need to check if our scenario is in agreement with existing gamma-ray observations, although there is no gamma-ray limit in the literature for dark matter decaying into right-handed neutrinos. Thus, in order to estimate if our best-fit points are then consistent with gamma-ray bounds, we looked after the popular decay channels to check which ones produce similar gamma-ray spectra. They are all different, but the ones that resemble most our case are the decay into WW and $W\ell$. To explicitly show our procedure, we chose a benchmark scenario with $M_N = 10, 50,$ and 80 GeV, where the best fit to the positron data is given by $M_{DM_1} \simeq 2000$ GeV and $M_{DM_2} = 300$ GeV. In order to get a comparable limit, we need to rescale the spectrum according to Fig. 10. We highlight that the WW and $W\ell$ spectra were rescaled by a different constant factor to approximate their spectra to ours. For example, for $M_{DM_1} \simeq 2000$ GeV and $M_N = 10$ GeV, we had to multiply our spectrum by 6. Therefore, the limits provided by Ref. [36] need to be suppressed also by a factor of 6 times to be applicable to our setup. Moreover, an additional factor

$1/2$ should be included due to the DM density, since in our case we have DM components. That said, the gamma-ray limit from Ref. [36] at face value reads 3.6×10^{28} s, but it should read as 3×10^{27} s. For $M_{DM_2} = 300$ GeV, at face value the limit reads 4.8×10^{27} s [36], but taking into account the factors provides 1.2×10^{27} s.

Using these estimates, we conclude that the lighter DM candidate is in agreement with the limits, while the heavier not by a factor of a few. Having in mind that the limits in Ref. [36] are optimistic due to the profile and target selected (inner galaxy) these gamma-ray bounds are subject to large uncertainties, we may argue that our best-fit points are marginally in agreement with the gamma-ray bounds. A similar reasoning could be applied to different benchmark points.

In addition, we emphasize that any assessment of the best-fit points relies on the background model assumed for the positron secondary production resulting from the collision of primary cosmic rays with the interstellar medium. In our work, we adopt the background model used by the AMS-02 Collaboration in their data release [18]; thus, our conclusions are based on that. There are other competitive gamma-ray bounds in the literature [38] which can also be relaxed in a similar way.

- [1] O. Adriani *et al.* (PAMELA Collaboration), An anomalous positron abundance in cosmic rays with energies 1.5–100 GeV, *Nature (London)* **458**, 607 (2009).
- [2] M. Ackermann *et al.* (Fermi-LAT Collaboration), Measurement of Separate Cosmic-Ray Electron and Positron Spectra with the Fermi Large Area Telescope, *Phys. Rev. Lett.* **108**, 011103 (2012).
- [3] M. Aguilar *et al.* (AMS Collaboration), First Result from the Alpha Magnetic Spectrometer on the International Space Station: Precision Measurement of the Positron Fraction in Primary Cosmic Rays of 0.5350 GeV, *Phys. Rev. Lett.* **110**, 141102 (2013).
- [4] I. Cholis and D. Hooper, Dark matter and pulsar origins of the rising cosmic ray positron fraction in light of new data from AMS, *Phys. Rev. D* **88**, 023013 (2013).
- [5] A. Ibarra, A. S. Lamperstorfer, and J. Silk, Dark matter annihilations and decays after the AMS-02 positron measurements, *Phys. Rev. D* **89**, 063539 (2014).
- [6] D. Hooper, C. Kelso, and F. S. Queiroz, Stringent and robust constraints on the dark matter annihilation cross section from the region of the Galactic center, *Astropart. Phys.* **46**, 55 (2013).
- [7] M. Ackermann *et al.* (Fermi-LAT Collaboration), Searching for Dark Matter Annihilation from Milky Way Dwarf Spheroidal Galaxies with Six Years of Fermi Large Area Telescope Data, *Phys. Rev. Lett.* **115**, 231301 (2015).
- [8] S. Galli, F. Iocco, G. Bertone, and A. Melchiorri, Updated CMB constraints on dark matter annihilation cross-sections, *Phys. Rev. D* **84**, 027302 (2011).
- [9] C. Weniger, P. D. Serpico, F. Iocco, and G. Bertone, CMB bounds on dark matter annihilation: Nucleon energy-losses after recombination, *Phys. Rev. D* **87**, 123008 (2013).
- [10] E. Nardi, F. Sannino, and A. Strumia, Decaying dark matter can explain the $e^+ - e^-$ excesses, *J. Cosmol. Astropart. Phys.* **01** (2009) 043.
- [11] A. Arvanitaki, S. Dimopoulos, S. Dubovsky, P. W. Graham, R. Harnik, and S. Rajendran, Astrophysical probes of unification, *Phys. Rev. D* **79**, 105022 (2009).
- [12] K. R. Dienes, J. Kumar, and B. Thomas, Dynamical dark matter and the positron excess in light of AMS results, *Phys. Rev. D* **88**, 103509 (2013).
- [13] C.-Q. Geng, D. Huang, and L.-H. Tsai, Imprint of multi-component dark matter on AMS-02, *Phys. Rev. D* **89**, 055021 (2014).
- [14] K. Belotsky, M. Khlopov, C. Kouvaris, and M. Laletin, Decaying dark atom constituents and cosmic positron excess, *Adv. High Energy Phys.* **2014**, 214258 (2014).
- [15] S. Profumo, Dissecting cosmic-ray electron-positron data with Occam’s Razor: the role of known Pulsars, *Central Eur. J. Phys.* **10**, 1 (2011).
- [16] D. Hooper, P. Blasi, and P. D. Serpico, Pulsars as the sources of high energy cosmic ray positrons, *J. Cosmol. Astropart. Phys.* **01** (2009) 025.
- [17] D. Grasso *et al.* (Fermi-LAT Collaboration), On possible interpretations of the high energy electron-positron spectrum measured by the Fermi Large Area Telescope, *Astropart. Phys.* **32**, 140 (2009).
- [18] M. Aguilar *et al.* (AMS Collaboration), Towards Understanding the Origin of Cosmic-Ray Positrons, *Phys. Rev. Lett.* **122**, 041102 (2019).
- [19] A. U. Abeysekara *et al.* (HAWC Collaboration), Extended gamma-ray sources around pulsars constrain the origin of the positron flux at Earth, *Science* **358**, 911 (2017).
- [20] Y. Farzan and M. Rajaei, Dark matter decaying into millicharged particles as a solution to AMS 02 positron excess, *J. Cosmol. Astropart. Phys.* **04** (2019) 040.
- [21] M. D. Campos, F. S. Queiroz, C. E. Yaguna, and C. Weniger, Search for right-handed neutrinos from dark matter annihilation with gamma-rays, *J. Cosmol. Astropart. Phys.* **07** (2017) 016.
- [22] B. Batell, T. Han, and B. Shams Es Haghi, Indirect detection of neutrino portal dark matter, *Phys. Rev. D* **97**, 095020 (2018).
- [23] G. B. Gelmini, S. Nussinov, and M. Roncadelli, Bounds and prospects for the Majoron model of left-handed neutrino masses, *Nucl. Phys.* **B209**, 157 (1982).
- [24] G. Gelmini, D. N. Schramm, and J. W. F. Valle, Majorons: A simultaneous solution to the large and small scale dark matter problems, *Phys. Lett.* **146B**, 311 (1984).
- [25] A. Santamaria, J. Bernabeu, and A. Pich, Neutrino masses, Majorons and muon decay, *Phys. Rev. D* **36**, 1408 (1987).
- [26] K. Choi and A. Santamaria, 17-KeV neutrino in a singlet-triplet majoron model, *Phys. Lett. B* **267**, 504 (1991).
- [27] V. Berezhinsky and J. W. F. Valle, The KeV majoron as a dark matter particle, *Phys. Lett. B* **318**, 360 (1993).
- [28] W.-F. Chang and J. N. Ng, Minimal model of Majoronic dark radiation and dark matter, *Phys. Rev. D* **90**, 065034 (2014).
- [29] F. S. Queiroz and K. Sinha, The Poker face of the Majoron dark matter model: LUX to keV line, *Phys. Lett. B* **735**, 69 (2014).
- [30] S. M. Boucenna, S. Morisi, Q. Shafi, and J. W. F. Valle, Inflation and Majoron dark matter in the seesaw mechanism, *Phys. Rev. D* **90**, 055023 (2014).
- [31] E. Ma and M. Maniatis, Pseudo-Majoron as light mediator of singlet scalar dark matter, *J. High Energy Phys.* **07** (2017) 140.
- [32] C. Garcia-Cely and J. Heeck, Neutrino lines from Majoron dark matter, *J. High Energy Phys.* **05** (2017) 102.
- [33] T. Brune and H. Ps, Massive Majorons and constraints on the Majoron-neutrino coupling, *Phys. Rev. D* **99**, 096005 (2019).
- [34] S. Ando and K. Ishiwata, Constraints on decaying dark matter from the extragalactic gamma-ray background, *J. Cosmol. Astropart. Phys.* **05** (2015) 024.
- [35] A. Massari, E. Izaguirre, R. Essig, A. Albert, E. Bloom, and G. A. Gmez-Vargas, Strong optimized conservative Fermi-LAT constraints on dark matter models from the inclusive photon spectrum, *Phys. Rev. D* **91**, 083539 (2015).
- [36] T. Cohen, K. Murase, N. L. Rodd, B. R. Safdi, and Y. Soreq, Gamma-ray Constraints on Decaying Dark Matter and Implications for IceCube, *Phys. Rev. Lett.* **119**, 021102 (2017).
- [37] Y. Gnolini *et al.*, Cosmic-ray transport from AMS-02 boron to carbon ratio data: Benchmark models and interpretation, *Phys. Rev. D* **99**, 123028 (2019).
- [38] S. Ando and K. Ishiwata, Constraining particle dark matter using local galaxy distribution, *J. Cosmol. Astropart. Phys.* **06** (2016) 045.